



MIT Open Access Articles

Athermal Operation of Silicon Waveguides: Spectral, Second Order and Footprint Dependencies

The MIT Faculty has made this article openly available. **Please share** how this access benefits you. Your story matters.

Citation	Vivek Raghunathan, Winnie N. Ye, Juejun Hu, Tomoyuki Izuhara, Jurgen Michel, and Lionel Kimerling, "Athermal operation of Silicon waveguides: spectral, second order and footprint dependencies," Opt. Express 18, 17631-17639 (2010)
As Published	http://dx.doi.org/10.1364/OE.18.017631
Publisher	Optical Society of America
Version	Author's final manuscript
Citable link	http://hdl.handle.net/1721.1/58117
Terms of Use	Attribution-Noncommercial-Share Alike 3.0 Unported
Detailed Terms	http://creativecommons.org/licenses/by-nc-sa/3.0/

Athermal operation of Silicon waveguides: spectral, second order and footprint dependencies

Vivek Raghunathan,¹ Winnie N.Ye,² Juejun Hu,¹ Tomoyuki Izuhara,³ Jurgen Michel,¹ and Lionel Kimerling¹

¹Microphotonics Center, Massachusetts Institute of Technology, Cambridge, Massachusetts 02139, USA

²Carleton University, 1125 Colonel By Drive, Ottawa, Ontario, Canada

³Enablance Technologies, 100 Fordham Road, Wilmington, MA-01887

*Corresponding authors: vivekr@mit.edu, lckim@mit.edu

Abstract: We report the design criteria and performance of Si ring resonators for passive athermal applications in wavelength division multiplexing (WDM). The waveguide design rules address i) positive-negative thermo-optic (TO) composite structures, ii) resonant wavelength dependent geometry to achieve constant confinement factor (Γ), and iii) observation of small residual second order effects. We develop exact design requirements for a temperature dependent resonant wavelength shift (TDWS) of 0 pm/K and present prototype TDWS performance of 0.5pm/K. We evaluate the materials selection tradeoffs between high-index contrast (HIC) and low-index contrast (LIC) systems and show, remarkably, that FSR and footprint become comparable under the constraint of athermal design.

©2010 Optical Society of America

OCIS codes: (130.2790) Guided waves; (130.3130) Integrated optics materials; (160.6840) Thermo-Optical Materials; (160.5470) Polymers; (230.5750) Resonators; (230.7370) Waveguides.

References and links

1. M.S. Rasras, D.M. Gill, S.S. Patel, K.Y. Tu, Y.K. Chen, A.E. White, A.T.S. Pomerene, D.N. Carothers, M.J. Grove, D.K. Sparacin, J. Michel, M.A. Beals, L.C. Kimerling, "Demonstration Of A Fourth-Order Pole-Zero Optical Filter Integrated Using CMOS Processes," *Journal Of Lightwave Technology* **25** (1), 87-92 (2007).
2. Y. Kokubun, S.Yoneda and S.Matsuura, "Temperature-independent optical filter at 1.55 μ m wavelength using a silica-based athermal waveguide", *Elec Lett.* **34**, 367-369 (1998).
3. Y. Kokubun, S.Yoneda and H.Tanaka, "Temperature-independent narrowband optical filter at 1.3 μ m wavelength by an athermal waveguide", *Elec Lett.* **32**, 1998-2000 (1996)
4. Sai T. Chu, Wugen Pan, Shuichi Suzuki, Brent E. Little, Shinya Sato, and Yasuo Kokubun, "Temperature Insensitive Vertically Coupled Microring Resonator Add/Drop Filters by Means of a Polymer Overlay", *IEEE Photonics Technol. Lett.* **11**,1138-1140 (1999)
5. Jong-Moo Lee, Duk-Jun Kim, Hokyun Ahn, Sang-Ho Park, and Gyungock Kim, "Temperature Dependence of Silicon Nanophotonic Ring Resonator with a Polymeric overlayer", *J. Lightwave Tech.* **25**, 2236-2243 (2007)
6. Jong-Moo Lee, Duk-Jun Kim, Gwan-Ha Kim, O-Kyun Kwon, Kap-Joong Kim, and Gyungock Kim, "Controlling temperature dependence of silicon waveguides using slot structure", *Opt. Express* **14**, 1645-1652 (2008)
7. Jie Teng, Pieter Dumon, Wim Bogaerts, Hongbo Zhang, Xigao Jian, Xiyou Han, Mingshan Zhao, Geert Morthier, Roel Baets, "Athermal Silicon-on-insulator ring resonators by overlaying a polymer cladding on narrowed waveguides", *Opt. Express* **17**, 14627-14633 (2009)
8. Biswajeet Guha, Bernardo B. C. KyotokuI, and Michal Lipson, "CMOS-compatible athermal silicon microring resonators", *Opt. Express* **18**(4), 3487-3493 (2010)

9. Huamao Huang, Seng-Tiong Ho, Dexiu Huang, Yongming Tu, and Wen Liu, "Design of temperature independent arrayed waveguide gratings based on the combination of multiple types of waveguide", *Appl.Optics*. **49(16)**, 3025-3034 (2010)
 10. W. N. Ye, J. Michel, and L. C. Kimerling, "Athermal high-index-contrast waveguide design," *IEEE Photonics Technol. Lett.* **20**, 882–884 (2008)
 11. Jacob T Robinson, Kyle Preston, Oskar Painter and Michal Lipson, "First principle derivation of gain in high-index contrast waveguides", *Opt. Express* **16**, 16659-16669 (2008)
 12. G. Ghosh, *Handbook of Thermo-Optic Coefficients of Optical Materials with Applications* (Academic, 1998).
 13. J. Hu, X. Sun, A. Agarwal, and L. C. Kimerling, "Design guidelines for optical resonator biochemical sensors", *J. Opt. Soc. Am. B.* **26**, 1032-1041 (2009)
 14. G. Cocorullo ,F.G. Della Corte,L. Moretti ,I. Rendina and A. Rubino, "Measurement of the thermo-optic coefficient of a-Si:H at the wavelength of 1500 nm from room temperature to 200°C", *J. Non-Crystalline Solids*, **299–302** , 310–313 (2002)
 15. N.-N Feng, G.-R. Zhou, C. Xu, and W.-P. Huang, "Computation of full-vector modes for bending waveguide using cylindrical perfectly matched layers," *J. Lightwave Technol.* **20(11)**, 1976-1980 (2002)
-

1. Introduction

Silicon is a compelling material choice for electronic and photonic applications using CMOS fabrication technology and requiring seamless electronic-photonic integration. The resulting performance benefits of improved power efficiency, increased functionality, enhanced reliability, and reduced cost provide strong incentives for on chip electronic-photonic integration. However, high levels of device integration create significant local and global chip temperature excursions during operation that prove problematic for silicon-based photonics due to the high thermo-optic coefficient of silicon. In particular, thermo-optic (TO) index variations will induce temperature dependent wavelength shifts (TDWS) of resonant devices that limit wavelength resolution in applications such as wavelength division multiplexing (WDM) and high-resolution spectroscopy. Active thermal compensation by heaters and thermo-electric coolers are the legacy solution for low-density integration. In fact, the silicon CMOS layered architecture was shown recently to be ideal for embedded thermo-optic phase shifters for tuning complex filters [1]. However, the required electrical power and the number of I/O lines ultimately limit integration density. Passive thermo-optic compensation of silica photonic devices by a negative thermo-optic polymer cladding (PMMA) was first reported by Kokubun et al. [2-4]. Lee et al. [5,6] have extended the application of compensating polymer claddings to silicon ring resonators and have exhibited significant thermo-optic compensation to a TDWS of 2pm/K. Teng et al. [7] used a similar approach for SOI rings with a polymer top-cladding. Guha et al. [8] and Huang et al. [9] have employed alternate device design solutions to overcome the thermal dependence in interference-based devices. We have recently shown that exact athermal design is achievable for both symmetric and asymmetric waveguide-cladding geometries [10]. This communication reports the application of those design principles with the creation of prototypes that exhibit reproducible TDWS = 0.5pm/K for silicon-on-oxide ring resonators and reveal, with these devices, ultimate spectral, second-order and footprint constraints for athermal silicon waveguides.

2. Theory

2.1 Polymer over-cladding

The effective index (n_{eff}) of a waveguide system depends on the refractive index of the core (n_c) and the cladding (n_{cl}). For an asymmetric channel waveguide system, with a different top and bottom cladding, we can express the system thermo-optic coefficient [10,11] as

$$\frac{dn_{eff}}{dT}(\lambda) = \Gamma_c(\lambda) \frac{dn_c}{dT}(\lambda) + \Gamma_{tcl}(\lambda) \frac{dn_{tcl}}{dT}(\lambda) + \Gamma_{bcl}(\lambda) \frac{dn_{bcl}}{dT}(\lambda) \quad (1)$$

where $\frac{dn_{eff}}{dT}(\lambda)$ is the effective TO coefficient of the waveguide system at a given wavelength, while $\frac{dn_c}{dT}(\lambda)$, $\frac{dn_{tcl}}{dT}(\lambda)$ and $\frac{dn_{bcl}}{dT}(\lambda)$ represent the TO coefficients of the core, the top cladding and the bottom cladding respectively. Parameters $\Gamma_c(\lambda)$, $\Gamma_{tcl}(\lambda)$ and $\Gamma_{bcl}(\lambda)$ in the above equation represent the confinement factor of the core, the top and bottom cladding respectively as defined by Robinson et al.[11]. Henceforth, in all of our formulations, we shall consider only the effect of top cladding on the TO coefficient of the system. This assumption is justified in the case of SiO₂ as the bottom cladding, since its TO coefficient is an order of magnitude less than that of the Si waveguide and the polymer top clad as shown in Table 1. Eq.(1) is a first order approximation of the refractive index variation with temperature where we ignore the variation of $\Gamma(\lambda)$ with temperature and the second order variation of the refractive index of the core and cladding. We assume that the thermal expansion coefficient of the substrate doesn't change the geometry of the channel waveguide and hence the confinement factor in the given temperature range. Also note that we have assumed that the thermo-optic coefficient of the core and the cladding do not vary with wavelengths, since a-Si, SiO₂, and polymers do not have any dispersion in the wavelength near the IR region.

Athermal operation of a waveguide system is defined by the condition of $\frac{dn_{eff}}{dT}(\lambda)=0$, which from Eq.(1) can be reached only if the cladding has a negative thermo-optic coefficient. Motivated by this theory, we use polymer cladding for Si waveguides, as polymers are known to have a negative thermo-optic coefficient. The high thermo-optic coefficient of a-Si (Table 1) requires selection of polymers with an equally high thermo-optic coefficient. Many commercially available polymers have TO coefficients [12] smaller than a-Si. We use a proprietary hyperlinked fluoropolymer recently developed by Enablence (EP) that has been designed to have a high $dn/dT = -2.65 \times 10^{-4} \text{ K}^{-1}$ and a refractive index of 1.3793 at 1550nm.

Table 1. Refractive index and TO coefficient of materials in this study

Material	a-Si	SiO ₂	Si ₃ N ₄	EP
n (@1550nm)	3.48	1.46	2.05	1.3793
dn/dT ($\times 10^{-4} \text{ K}^{-1}$)	2.3	0.1	0.4	-2.65

2.2 Wavelength dependence and second order effects

In Eq. (1), note the dependence of $\frac{dn_{eff}}{dT}(\lambda)$ on wavelength arising due to the variation of confinement factor with wavelength. In other words, we would expect $\Gamma(\lambda)$ to decrease with increasing wavelength owing to the longer evanescent tail. This dependence proves even more crucial for waveguides of dimensions 700nm×216nm, as we are studying wavelengths in the near IR regime (1450nm -1550nm) whose magnitude in the core is comparable to the core dimension. The single mode confinement required for ring resonators carries the important consequence that athermal operation can be achieved at only one wavelength for a given waveguide dimension.

The variation of confinement factor with wavelength influences the effective TO coefficient, which in turn manifests as a dependence of TDWS ($\frac{d\lambda_r}{dT}$) on wavelength. TDWS can be related to the effective TO coefficient using Eq.(2).

$$\frac{1}{\lambda_r} \frac{d\lambda_r}{dT}(\lambda) = \frac{1}{n_g} \frac{dn_{eff}}{dT}(\lambda) \quad (2)$$

It is more practical to simulate TDWS, as opposed to the effective system TO coefficient, because TDWS is the experimental observable. Furthermore, fine wavelength resolution (roughly 1pm) and hence very high refractive index measurement accuracy may be achieved through a resonant peak fitting algorithm [13].

Our model predicts a decrease in effective thermo-optic coefficient with increasing resonant wavelength due to the resulting decrease of $\Gamma(\lambda)$. As the propagating wavelength increases at constant waveguide dimension, the effective TO contribution from the cladding increases. The slope (rate of TO change) for the polymer clad structure is higher than for the the oxide clad structure, because the magnitude of the thermo-optic coefficient of polymer EP is higher than for the oxide. It is apparent from Eq. (1) that the slope will be larger for the EP polymer cladding as the contribution from the second term becomes significant. For a TM mode, Γ varies significantly by changing the height of the waveguide. With an appropriate polymer cladding, a true athermal operation (i.e. TDWS=0) can be achieved for a thin waveguide due to the reduced confinement and greater expansion of the mode into the cladding regime.

Any residual second order terms should become significant when the first order terms vanish according to $\frac{dn_{eff}}{dT}(\lambda) = 0$ at very small resonance shifts (<2pm/K). It is a reasonable assumption that the resonant wavelength shifts linearly with temperature, and it is largely governed by Eq. (1) and Eq. (2). Such linear relations hold true for relatively large peak shifts (>10pm/K). However at extremely small wavelength shifts, the second order contributions arising from the variation of Γ with temperature and possibly the second order contribution from the refractive index become significant and cannot be neglected. In theory, with increase in temperature, the refractive index of the core increases and that of the polymer cladding decreases, thereby increasing the confinement factor resulting in a larger peak shift. Thus the refractive index variation including the second order term can be written as follows

$$\begin{aligned} dn_{eff}(n_c, n_{cl}) = & (\Gamma_c \cdot \frac{\partial n_c}{\partial T} + \Gamma_{cl} \cdot \frac{\partial n_{cl}}{\partial T}) \cdot dT \\ & + \frac{1}{2} \cdot [\Gamma_c \frac{\partial^2 n_c}{\partial T^2} + \Gamma_{cl} \frac{\partial^2 n_{cl}}{\partial T^2} + \frac{\partial \Gamma_c}{\partial n_c} (\frac{\partial n_c}{\partial T})^2 + \frac{\partial \Gamma_{cl}}{\partial n_{cl}} (\frac{\partial n_{cl}}{\partial T})^2 + \frac{\partial \Gamma_c}{\partial n_{cl}} \frac{\partial n_c}{\partial T} \frac{\partial n_{cl}}{\partial T} + \frac{\partial \Gamma_{cl}}{\partial n_c} \frac{\partial n_c}{\partial T} \frac{\partial n_{cl}}{\partial T}] \cdot dT^2 \end{aligned} \quad (3)$$

where Γ_c and Γ_{cl} are the confinement factor of the core and the cladding (only the polymer top cladding is considered), respectively. The second order terms can be categorized into two types of contributions:

- 1) the term $\frac{1}{2} \cdot (\Gamma_c \frac{\partial^2 n_c}{\partial T^2} + \Gamma_{cl} \frac{\partial^2 n_{cl}}{\partial T^2})$ corresponds to the second order TO coefficients of the core and cladding materials;
- 2) the term $\frac{1}{2} \cdot [\frac{\partial \Gamma_c}{\partial n_c} (\frac{\partial n_c}{\partial T})^2 + \frac{\partial \Gamma_{cl}}{\partial n_{cl}} (\frac{\partial n_{cl}}{\partial T})^2 + \frac{\partial \Gamma_c}{\partial n_{cl}} \frac{\partial n_c}{\partial T} \frac{\partial n_{cl}}{\partial T} + \frac{\partial \Gamma_{cl}}{\partial n_c} \frac{\partial n_c}{\partial T} \frac{\partial n_{cl}}{\partial T}]$ represents the TDWS due to the variation of confinement factors at different temperatures.

2.3 Design and fabrication constraints: TE mode vs TM mode

The design leverage of the passive approach outlined above is that athermal operation is achieved universally for a particular confinement factor resulting from a selected core-polymer cladding system (Eq. (1)). This confinement factor is however reached for different waveguide dimensions for TE and TM modes. For example, reduction of the confinement factor is achieved by reducing the waveguide width for TE mode and by reducing its height for TM mode. Thus, without any loss of generality, one can safely claim that the physics behind the behavior of TE and TM mode is similar as long as one tailors the waveguide design to have the same confinement factor for each mode. The proof-of-concept prototypes in the experimental section of this paper to follow are designed for exclusive TM mode propagation. The lithographic constraints of our fabrication facility allow a minimum waveguide width of 700nm and adequate mode penetration into the upper polymer cladding is accomplished by the use of a-Si waveguides of reduced thickness. The a-Si ring resonators have racetrack configurations with radii of 20 microns, where the bending loss (7.84×10^{-4} dB/cm) of TM mode is insignificant. Furthermore, the loss of these devices is largely governed by the scattering loss which is smaller for the TM mode than the TE mode. Owing to the high loss and low evanescent coupling coefficient associated with the TE mode, we do not resolve resonant peaks in the TE polarization transmission spectra, and the presented performance data are for the TM polarization. We demonstrate that TM mode propagation can achieve athermal operation at relatively wider waveguide widths and smaller thickness. However, the governing theory and the design rules apply equally well for TE mode.

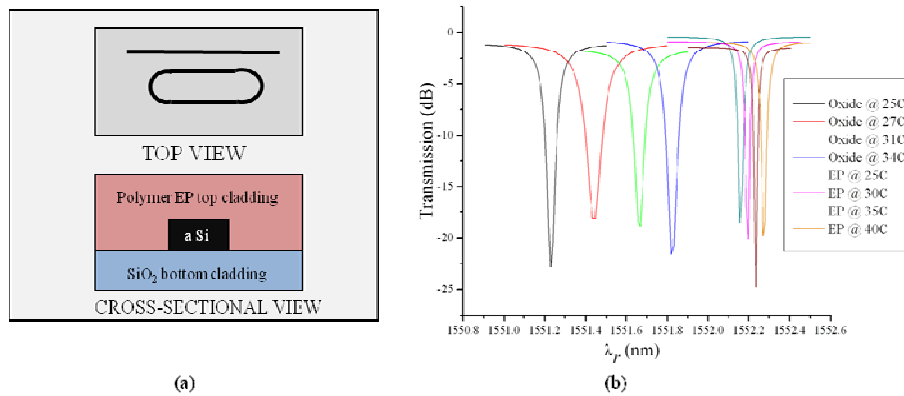


Fig.1. (a) Schematic view of an a-Si racetrack resonator and (b) the transmission spectra showing the resonance peak shift with temperature for both oxide clad and polymer clad devices. We compare a-Si rings of the same cross-section ($700\text{nm} \times 216\text{nm}$) and different top claddings (oxide and polymer). In the case of an oxide clad ring, the positive TO coefficient of both core and cladding result in a positive peak shift of 63pm/K. There is significant TO compensation for the polymer clad ring and the peak shift is reduced to 7pm/K for this waveguide design.

3. Prototype fabrication

We fabricated a-Si ring resonators with a racetrack configuration (Fig. (1a)) via photolithography using an i-line stepper. We deposited two sets of a-Si films, one with thickness of 206nm and other with 216nm. The actual dimensions of the waveguides are measured to be $700\text{nm} \times 216\text{nm}$ and $700\text{nm} \times 206\text{nm}$. Both waveguides are designed to operate at single mode for TM polarization. We deposited a CVD (chemical vapor deposition) oxide film on one set of waveguides to be used as a reference; while the other sets of devices were

spun with a hyperlinked fluoropolymer sample, EP, at Enablence Inc. The spin coating process was followed by UV exposure after which the samples are baked in vacuum for around 8 hrs to cross-link the EP polymer. We then measure the TM mode transmission spectrum at various temperatures to monitor the resonant peak positions and their thermo-optic induced changes.

4. Prototype performance

Fig. (1b) shows the transmission spectra comparing the performance of oxide over-cladding and EP over-cladding at various temperatures. The glass transition temperature of EP lies below room temperature and hence outside the operating range of our interest (25-125°C). We thus neglect the higher order variations due to the polymer glass transition in our experiments. We measure the resonant wavelength shift for the oxide and polymer clad waveguides over a range of temperatures as is shown in Fig. (2).

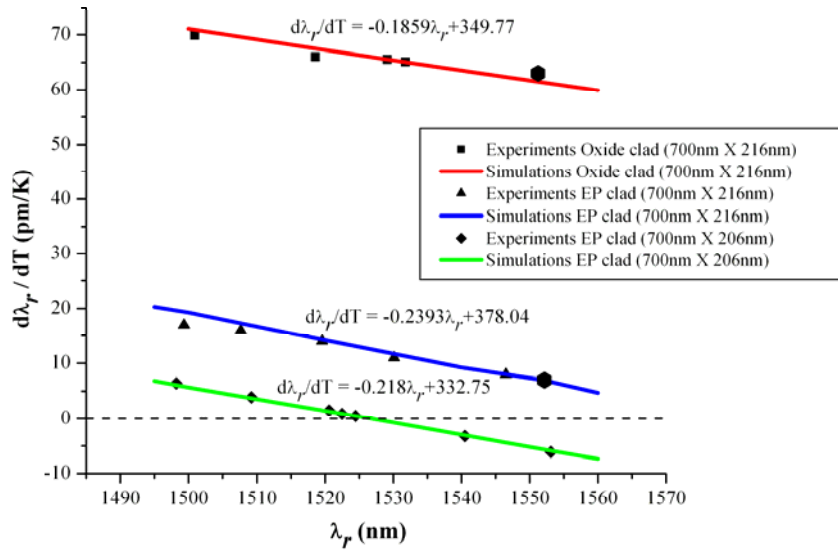


Fig. 2. Experimental results showing $d\lambda_r/dT$ variation with λ_r for TM mode propagation. The slope of the $d\lambda_r/dT$ variation with λ_r reflects the role of Γ (see Eqn. (1), (2)) on TO and $d\lambda_r/dT$. Hence the wavelength at the dashed-line crossover point is a unique condition for $d\lambda_r/dT = 0$. The hexagonal bold data points correspond to the spectral data shown in Fig. (1)

Fig. (2) expresses the effects of both thermo-optic coefficient of the cladding and confinement factor on the resonance shift. The measurements for each resonant wavelength were carried out between 25°C-60°C and every data point is a linear regression of 8 data points taken at every 5°C interval. For large resonance shifts (TDWS > 10pm/K), $R^2 \geq 0.99$, and for near athermal performance (TDWS \leq 1pm/K) $R^2 \geq 0.94$ due to reduced linear correlation arising from the residual second order terms discussed below. The dramatic decrease of TDWS from 65 pm/K for an oxide cladding to as low as 0.5pm/K at 1524nm for the EP polymer cladding can be attributed to the negative thermo-optic coefficient of the polymer and its effect on the effective thermo-optic coefficient of the system. Figure 2 demonstrates two important results: i) the achievement near perfect thermo-optic

compensation, and ii) a variation of TDWS with wavelength that correlates well with simulated values. As explained earlier and as verified by the coincidence between data and simulation, the variation in confinement factor with wavelength changes the TDWS. The excellent agreement between experimental data and the simulations clearly validates our theoretical formulation of TDWS in Section 2.

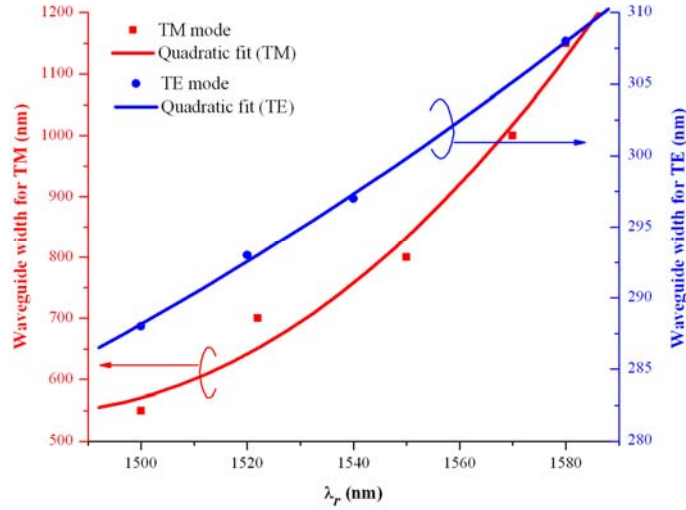


Fig. 3. Variation of athermal waveguide width with wavelength for TE and TM modes. These simulation results are for an a-Si waveguide of 206nm height with an SiO₂ underclad and the EP polymer over-cladding. The desired waveguide width for athermal operation increases with wavelength to keep the confinement factor constant, consistent with the theory presented in section 2.2.

The wavelength dependence of TDWS imposes an additional design constraint of different waveguide dimensions for different resonant wavelengths to achieve athermal operation. For a single WDM implementation, the mask design should incorporate varying waveguide widths, for instance, when the height of the waveguide (layer thickness) is fixed. Figure 3 plots the range of the wavelength dependent variation in waveguide dimensions for athermal operation of both TE and TM modes. The simulation assumes an a-Si ring with an oxide under-cladding and a polymer over-cladding. We fix the height of the a-Si waveguide at 206nm and calculate the desired width, to achieve a peak shift of less than 0.5pm/K, at various wavelengths. The desired width varies from 550nm (at 1500nm) to 1150nm (at 1580nm) as the wavelength increases. Such a large variation in waveguide width can be correlated to the small dependence of the confinement factor of a TM mode on width compared to height variation. Conversely, one can expect to achieve athermal operation of a TE mode over a smaller range of widths for a given range of wavelengths. Fig. (3) clearly shows this stronger dependence of confinement factor of a TE mode on the width of the waveguide. Fig. (3) also defines the ‘athermal constraint’ on fabrication tolerance, since changes in the waveguide width can shift athermal operation to a different wavelength. As an example, an error of 100nm in the waveguide width would shift the “athermal response peak” by 10nm.

Residual second order variations are revealed when TDWS is small. Fig. (4) shows the experimental variation of resonant wavelength with temperature for a 700nm × 206nm a-Si waveguide with an EP cladding.

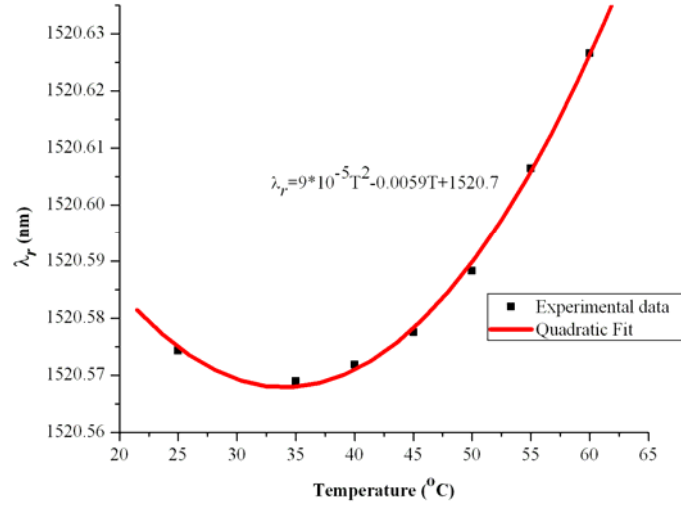


Fig. 4. Measured second order variations of resonant wavelength with fit to a quadratic dependence. The residual second order effects become important when the first order terms vanish at low peak shifts (<2pm/K). The quadratic term has contributions from the temperature dependence of the confinement factor and from the second order material coefficients.

The residual quadratic term seen in experiments ($9 \times 10^{-5} \pm 1 \times 10^{-5} \text{ nmK}^{-2}$) is of the same order of magnitude predicted in the simulation ($2 \times 10^{-5} \pm 1 \times 10^{-6} \text{ nmK}^{-2}$). The higher value of the experimental second order term compared to simulation suggests a significant contribution from the second order material coefficients, $\frac{\partial^2 n_c}{\partial T^2}$ and $\frac{\partial^2 n_{cl}}{\partial T^2}$, that we neglected in the simulations (first 2 second order terms in Eq. (3)). The first 2 second order terms of Eq. (3) can be calculated based on our the experimentally measured second order term, and a value of $4 \times 10^{-7} \pm 1 \times 10^{-7} \text{ K}^{-2}$ for the second order material coefficient of the waveguide system (in other words, second order effective material TO coefficient) results. Cocorullo et al. [14] have reported that the second order thermo-optic coefficient of a-Si is roughly $1.43 \times 10^{-6} \text{ K}^{-2}$, so the determined value is in a reasonable range for the polymer clad system.

5. Material selection for high density integration: Si rings vs Si₃N₄ rings

The motivation behind using Si ring resonators for WDM filter applications arises from its high-index contrast and high mode confinement. As a result, Si rings can have small bending radii resulting in large FSR. However, athermal operation of these rings requires reduced confinement ($\Gamma=0.58$) for the mode to penetrate the cladding. The result is a lower effective index (1.78) waveguide with higher radiative bending loss. This design rule leads one to inquire whether a lower-index contrast (LIC) waveguide core material with a lower TO coefficient, such as Si₃N₄ ($\text{TO}=4 \times 10^{-5}$), would perform as well or better for athermal WDM applications. We use bend radius (R_b) as a variable in the figure of merit for the ring resonator, and we calculate for TM mode to be consistent with our experimental results. We start the comparison by finding the confinement factor required for athermal operation of nitride rings with the same polymer cladding used for a-Si rings. We then proceed to find the bending radius for both Si and Si₃N₄ for a given bending loss [15], which we fixed at 4.34dB/cm (or 1 cm^{-1}).

Table 2 summarizes R_b for both systems. As the results show, the advantage of high-index contrast (HIC) (a-Si) is neutralized under the constraint of athermal operation, and the R_b performance is similar to the lower-index Si_3N_4 core. Therefore, materials selection of lower index contrast systems like Si_3N_4 might prove advantageous, since the lower TO coefficient may allow the use of a wider range of commercially available polymers to achieve athermal behavior. Si_3N_4 rings have a higher FSR due to their smaller group index (n_g), and they could prove additionally useful for athermal WDM applications where FSR is the primary performance driver. When developing scaling rules for the material selection for athermal performance, it is important to realize that HIC systems lose their benefits over LIC systems in terms of small R_b and high FSR, and the two performances becomes comparable.

Table 2. Performance comparison of two athermal waveguide designs, for an a-Si core and a Si_3N_4 core, with the same EP polymer overclad

Material	n	Γ	n_{eff}	n_g	$R_b(\text{microns})$
Si	3.48	0.58	1.78	3.68	3.5
Si_3N_4	2.05	0.9	1.75	2.2	5.5

6. Summary and conclusion

We develop the design principles for athermal waveguide device performance. We demonstrate prototype ring resonators with near complete thermo-optic compensation of an a-Si on SiO_2 waveguide using a polymer cladding. We measure a resonant wavelength shift of 0.5pm/K, which is the lowest TDWS value reported to date for silicon resonators. The design formalism and prototypes establish the requirement for a unique waveguide dimension for each operating wavelength. The athermal resonator performance reveals residual second order terms that are also described in the theoretical section. This report validates a general solution for temperature-independent performance of silicon resonant photonic devices. An evaluation of the performance tradeoffs of athermal HIC systems in terms of FSR and bend radius shows that LIC systems might be superior to HIC systems in certain applications.

Acknowledgement

We acknowledge Dr. Ningning Feng of Kotura for support with simulations for bending loss calculations. This work is sponsored under the Defense Advanced Research Projects Agency's Athermal Photonic Circuits (APhocs) program. The program is executed by the Microsystems Technology Office (MTO) under Award No. W911NF-09-1-0059, Program manager: Mike Haney.